Proceeding *20th SEAGC - 3rd AGSSEA Conference in conjunction with 22nd Annual Indonesian National Conference on Geotechnical Engineering.* Jakarta - INDONESIA, 6 -7 November 2018. ISBN No. 978-602-17221-6-9

3D Finite Element Analysis of Deep Excavation in Central Jakarta using Total and Effective Shear Strength Properties

Tatag Yufitra Rus[1], Bin-Chen Benson Hsiung[2] and Kuo-Hsin Yang[3]
[1]*Department of Civil and Construction Engineering, National Taiwan University of Science and Technology, Taipei, Taiwan*
[2]*Department of Civil Engineering, National Kaohsiung University of Science and Technology, Kaohsiung, Taiwan*
[3]*Department of Civil Engineering, National Taiwan University, Taipei, Taiwan*
E-mail: tatagyufitrarus@gmail.com

ABSTRACT: This paper presents a study on 3D finite element analysis of a large-scale deep excavation in Central Jakarta. The soil, Central Jakarta clay, is modeled by both Hardening Soil and Mohr-Coulomb model in Plaxis 3D. The total and effective stress analyses under undrained conditions were used to model the short-term undrained conditions of the clay during excavation. The input soil properties were established using data based on an extensive site investigation program including in situ and laboratory tests, and empirical relationships with standard penetration numbers (SPT-N). The top-down construction method and a supporting system of concrete slabs are also considered in the numerical model. The numerical results are compared with measured wall deformation from inclinometers at a certain distance from the corner of excavation. The simulations using drained and undrained soil shear strength (Undrained A and B functions in Plaxis 3D) are also compared and discussed.
Keywords: Jakarta, deep excavation, 3D finite element, total and effective stress analysis, wall deformation.

1. INTRODUCTION

Jakarta is the capital city of Indonesia has a population of more than 10 million continues to increase every year. The increase in population in Jakarta would be directly proportional to the need of the increase in infrastructure services in Jakarta and use of deep excavation is expected to be an essential scheme for private or public sectors. The role of the deep excavation in Jakarta is thus becoming important.

The wall displacement induced by deep excavation is the critical factor in designing the deep basement. However, limited references to high-quality soil properties data and few of the large-scale deep excavations that have been studied are the challenges in Central Jakarta. Moreover, most of the valuable information obtained is documented by the local language which raises the difficulty of deep excavation research in Central Jakarta.

The 3D FE analysis is technically used to study 3D wall behavior by the concept of corner effect which was first proposed by Ou *et al*. (2006) to indicate the location of the plane-strain of the diaphragm wall. The study of PSR for the Central Jakarta has been established using Undrained B (Hsiung *et al*. 2018) and was evaluated by comparing the result with using Undrained A to examine the reliable effective stress parameter in Central Jakarta clay.

This paper presents a well-documented case of large-scale deep excavation in Central Jakarta clay using total and effective stress parameter by 3D FE analysis. The excavation is practically completely placed in the thick layer of Central Jakarta clay. Detailed information corresponding to the structure details, soil conditions, in situ and laboratory soil tests, construction sequences, and monitoring data are introduced. The input soil properties were established using data based on an extensive site investigation program including in situ and laboratory tests, and empirical relationships with standard penetration numbers (SPT-N) and laboratory Triaxial tests. The results of numerical analysis by Plaxis 3D are also compared with previous results of Undrained B conducted by Hsiung *et al*. (2018) and discussed with the field measurement data to obtain the reliability of the parameters that were used in the simulations.

2. PROJECT DESCRIPTION AND SITE EXPLORATION

2.1 Details of excavation site condition

A deep excavation in Central Jakarta was selected for the case study and numerical analysis. Figure 1 shows the cross-section of this study. The construction was performed using a top-down method with five excavation stages, supported by four-level reinforced concrete slabs with various thicknesses. The maximum excavation depth was 19.03 m in the final excavation stage. The excavated pit was retained using a 1.0 m thick and 24.2 m deep diaphragm wall.

To raise the stiffness of the retaining wall, 414×405×18×28 steel h-beams were designed as the kingposts in the middle of the excavation area at 3.0 m intervals. The function of kingpost is to hold the weight of reinforced concrete slabs. The h-beams were inserted 4.0 m into bored piles with a diameter of 1.0 m and an embedded length of 14.5 m.

The diaphragm wall and kingposts were constructed before the soil was excavated to ground level (GL) −1.5 m. In the next phase, a deck slab with a thickness of 0.4 m was installed. The second excavation stage involved removing the soil to GL −5.28 m and then constructing a top slab at GL −3.88 m. Subsequently, the soil was excavated to GL−11.38 m and a middle slab with a thickness of 0.4 m was placed at GL−10.38 m. The fourth and fifth excavations were excavated after the middle slab installed. In the last construction stage, the bottom slab with a thickness of 1.0 m was installed at GL−17.73 m. Table 1 details the construction phases and time sequences of the excavation for this study.

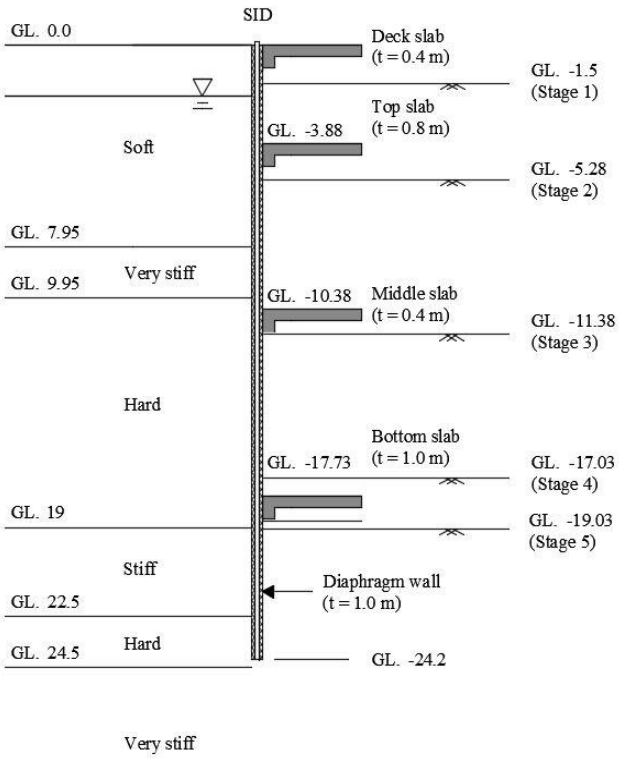

Figure 1 Cross-section and soil profile of the excavation

Table 1 Stage construction of the excavation

Stages	Construction sequences	Elapsed days
1	Diaphragm wall installation	101
2	1st excavations to the depth of GL. −1.5m	18
3	Deck slab installation at ground level (slab thickness, t=0.4 m)	20
4	2nd excavation to the depth of GL. −5.08m	30
5	Top slab construction at GL. −4.18m (slab thickness, t=0.8 m)	14
6	3rd excavation to the depth of GL. −11.18m	22
7	Middle slab construction at GL. −10.48m (slab thickness, t=0.4 m)	20
8	4th excavation to the depth of GL. −17.53m	28
9	5th excavation to the depth of GL. −18.93m	28
10	Bottom slab construction at GL. −18.13m (slab thickness, t=1.0 m)	21

2.2 In situ observation and instrumentation

Several monitoring instruments were installed around the excavation site, including inclinometers, surface settlement points, observation wells, rebar stress transducers, and kingpost strain gauges to monitor wall displacement during construction. The observation well summarized the groundwater level generally located at depth 2 m beneath the ground inside the excavation zone. Then, all monitoring data were carefully monitored to obtain the reliable and representative data were chosen for this study. However, only the representative measurement from inclinometer would be presented. The inclinometers were inserted on the left and right sides of the diaphragm wall. Figure 2 shows the locations of the inclinometers in the excavation area used for further discussion and analysis.

Some methods have been suggested for the correction of inclinometer readings to overcome wall toe movement. Inclinometer readings can be corrected by referring to the lateral movement at the B1F level during each excavation process as suggested by Hwang and Moh. (2007) & Hsiung and Hwang. (2009). This method considers the increment of the inclinometer reading at the specific point (i.e., the B1F level) for each excavation phase has a positive value, showing that the wall at the certain point regularly moves forward (toward the excavation site).

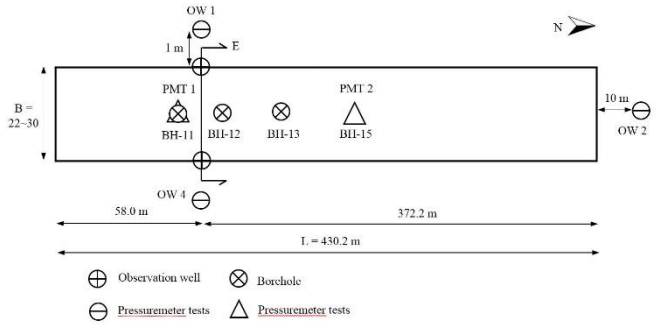

Figure 2 Plan view of the excavation (Hsiung *et al*. 2018)

The inclinometer readings may show a negative value if the inclinometer is embedded in the wall toe movement moves toward the retained soil side. Under those conditions at each excavation phase, all wall deflection reading curve must be corrected in parallel so that the wall deflection curve at the certain point can return to the same magnitude at previous excavation phase. Figure 3 and 4 present field measurement of lateral wall deformation before and after correction.

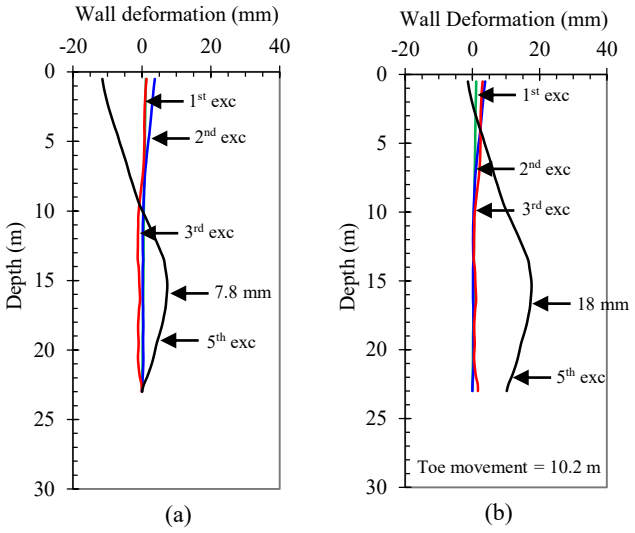

Figure 3 Monitoring data of wall deformation DW-15 (a) before correction; (b) after correction

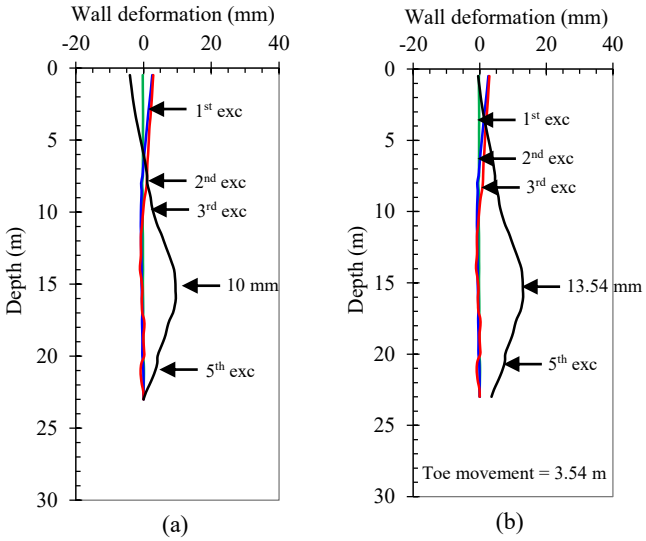

Figure 4 Monitoring data of wall deformation DW-171 (a) before correction; (b) after correction

2.3 Soil exploration

2.3.1 In situ and laboratory soil tests

Geotechnical characteristics of Central Jakarta soil data was obtained in underground section CP106 included in situ and laboratory tests. The site exploration work included 10 Boreholes (BHs), Standard Penetration Tests (SPT) and shear wave velocity (S-Wave velocity) located nearby each Section of the excavation as shown in Figure 7. Profile of soil characterization in Central Jakarta is displayed in Figure 6.

The soil in Central Jakarta is mainly dominated by clay/silt consisted of soft clay to very stiff clay as shown in Figure 6 (a) and (b). The soil is simplified as 2 layers which are upper soil layer and lower soil layer as shown in Table 2 and 3. Upper soil layer is from the ground surface to 7.95 m deep beneath the subsurface and continued by lower soil layer to hard soil layer at a depth of 40 m. Moreover, the soil unit weight is divided into two, 14 kN/m^3 and 18 kN/m^3 as detailed in Table 2 and 3.

Figure 6 (d) displays the relationships of the natural water content (ω) and the Atterberg Limit test results corresponding to depth. The natural water content was in the value range of 34.6–89.3% and was

close or higher than the plastic limit, with a liquidity index (*LI*) of 0.19–0.63. A gradual decrease in the *LI* relating to depth was also observed in this excavation, suggesting that shear strength may rise with depth. A high void ratio was connecting with the high water content as shown in Figure 6 (c), especially for the soil layer occupying top 10 m.

Permeability is one of the most significant index properties of soil in the advanced simulation of deep excavation. In situ permeability tests, by the falling head method, have been performed in selected boreholes (BH15-17). After firstly observing the initial level of the groundwater table, then the casing is loaded with water until achieving the top of the casing pipe. The water drop-down is measured at particular time intervals until attaining the stable or up to the first initial water level. The permeability test results represent that the hydraulic conductivity of the in-situ soil in the research Section is in the range of 3×10^{-8} to 7×10^{-8} m/s.

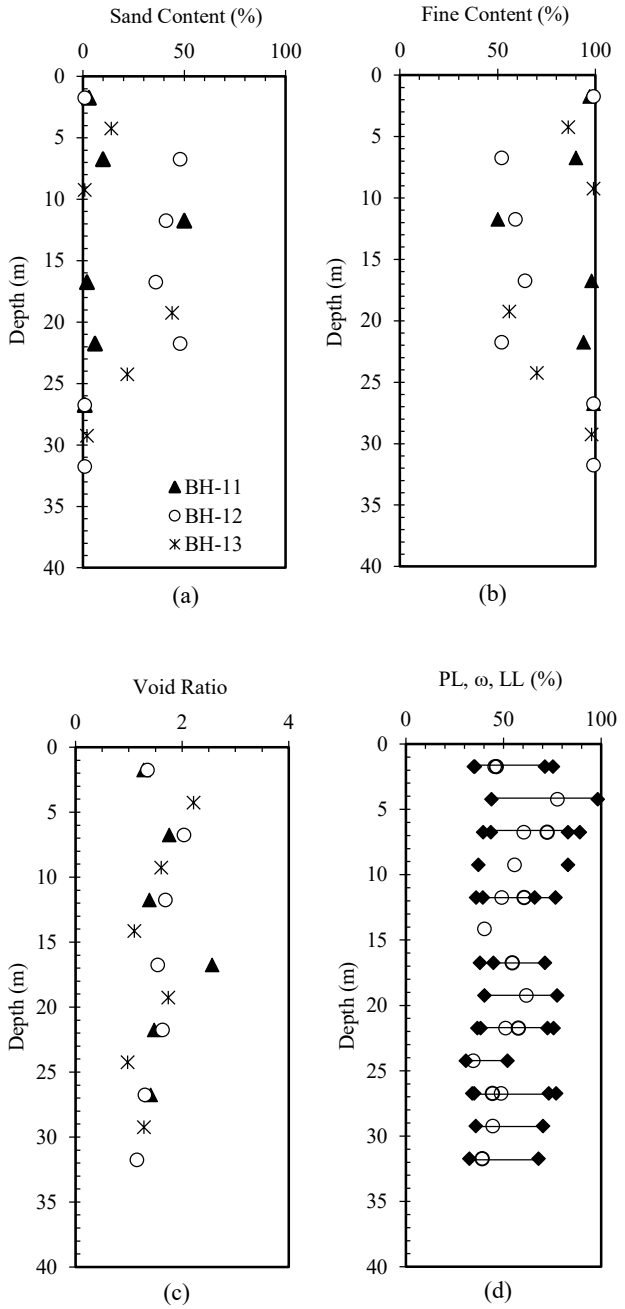

Figure 6 Profiles of borehole log information (a) Sand content; (b) Fine content; (c) Void ratio; (d) water content, plastic limit, and liquid limit (Hsiung *et al*. 2018)

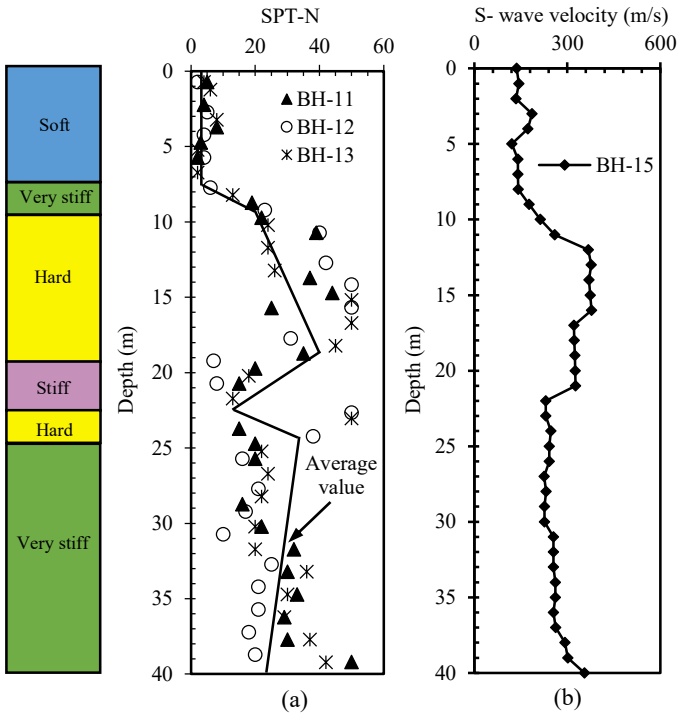

Figure 7 In-situ test information (a) SPT-N

The SPT-N value that was used in this study was the average value of BH-11, BH-12, and BH-13 due to close to the location of the excavation site. The N values remain lower than 10 to the depth of approximately 7 m below the surface and become stiffer reaching 50 to the depth of 13 m then consistently in the average of 30 from 20 to 40 m shown in Figure 7 (a). Moreover, the S-wave velocity curve line of BH15 looks similar the SPT-N curve value in the range from 136.4 m/s to 355 m/s displayed in Figure 7 (b). Those values support the classification of the soil layer into upper soil layer and lower soil layer.

2.3.2 Soil modulus and shear strength properties

The undrained shear strength (S_u) of the clay was collected from Triaxial CU tests and validated through several empirical methods for estimating the S_u of the clay. An empirical equation suggested by Muir Wood. (1983) correlates S_u with the *LI*. The empirical equation suggested by Muir Wood. (1983) is as follows.

$$S_u = 170 \times e^{-4.6LI} \text{ (kPa)} \quad (1)$$

Another empirical equation discussed in Hettiarachchi and Brown. (2009) associates the relationship of S_u with the SPT-N. The empirical equation suggested by Kulhawy and Mayne. (1990) is as follows.

$$S_u = 6 \times N \text{ (kPa)} \quad (2)$$

Figure 8 compares the S_u profile calculated from LI (the green shaded area), the SPT-N (red dash line), and the Triaxial UC test results (hollow circles). The S_u values obtained from these three methods display a similar trend. For depths of 15–30 m, the S_u value increased linearly with depth and could be approximated as 0.32 σ'_v (where σ'_v is the effective overburden pressure). For simplicity, the S_u of the soil for the numerical simulation was determined using Eq. (2) and the results are listed in Table 2. Regarding effective soil shear strength of clay, few high-quality, and reliable CU tests were delivered. Therefore, the effective friction angle of the soil that was selected in this research was simplified to upper layer 38° and lower layer 41° of effective friction angle as displayed in Table 3 for

Undrained A purposes. The K_0 values were defined by using equations from Jaky. (1944) for normally consolidated soils and from Mayne and Kulhawy. (1982) for overconsolidated soils, as shown in Eq. (3).

$$K_0(NC) = 1-\sin\phi' \quad (3a)$$

$$K_0(OC) = (1-\sin\phi')\, OCR^{(\sin\phi')} \quad (3b)$$

Where $K_0(NC)$ and $K_0(OC)$ are the at-rest earth pressure coefficient for normally consolidated and overconsolidated soils, respectively, ϕ' is the effective friction angle, and OCR is the overconsolidation ratio. The investigated clay reported that the soil is normally-consolidated clay to slightly over-consolidated clay. Therefore, the value of $K_0(NC)$ in Plaxis 3D follows the default setting by Jaky. (1994) equation.

The soil modulus measured from PMT was expected to be close to the initial soil modulus (E_i). For comparison, the measurements were converted to the soil modulus at 50% stress level (E_{50}) by using Eq. (4), assuming a hyperbolic curve for the stress-strain relationship.

$$E_{50} = E_i \frac{2-R_f}{2} \quad (4)$$

Where E_i is the initial soil modulus and R_f is the failure ratio, which is assumed to be 0.9 for clay. Figure 9 presents a comparison of E_{50} versus depth with various approaches and tests. As suggested by Hsiung. (2009) and Yong. (2015), the soil modulus for clay is E = 4000 N (kPa). Moreover, the Architectural Institute of Japan. (2001) suggested that E = 2800 N (kPa) can be applied to all soils. The E_{50} values determined from PMT appear located in between of those empirical equation values and become linearly associated with depth. The linear regression line for E_{50} obtained from PMTs is expressed as follows.

$$E_{50} = 833\,(z + 76)\ \text{(kPa)} \quad (5)$$

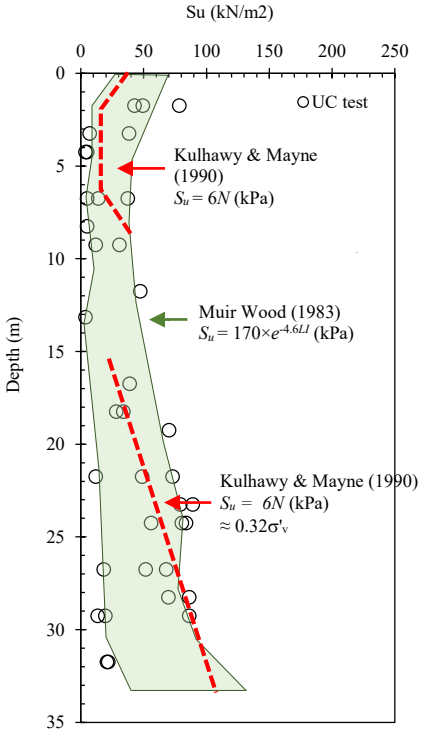

Figure 8 Undrained shear strength with depth (Hsiung *et al.* 2018)

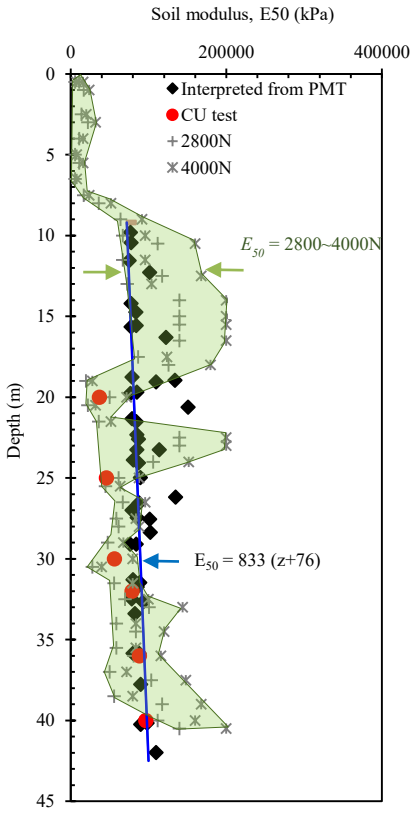

Figure 9 Undrained shear strength with depth (Hsiung *et al.* 2018)

Z indicates the soil depth in meters in Figure 9. The E_{50} values obtained from the CU tests tend to be at the lower bound of the E_{50} values compared to those determined using PMT and estimated from SPT-N (Figure 9). The low E_{50} values may have been attributable to the sample disturbance and the quality of the soil sample. Table 2 and 3 summarize the E_{50} values determined from PMT as shown in Eq. (5) as a soil parameter to be used in Undrained A and Undrained B for Hardening Soil and Mohr-Coulomb.

3. FINITE ELEMENT METHOD

3.1 Numerical analysis

A three-dimensional finite element (FE) analysis or benchmark analysis, was conducted to simulate the performance of the deep excavation in this research. The FE software Plaxis 3D was chosen as a numerical tool for the 3D simulations. Figure 11 displays the 3D FE model of the benchmark analysis. The dimension of the finite element model was 182 m×100 m×40 m. A half of excavation area with a length of 40 m was performed by symmetric model to represent the excavation case (E-E) which is located in the plane-strain condition of the excavation. This was because the influence of corner effects becomes inconsiderable once the distance is more than 30 m from the corner. At the distance of 30 m away from the corner, the wall is technically under plane-strain conditions and the wall deflection remains almost the same (Ou. 2006, Ou *et al.* 1996, and Hsiung *et al.* 2016). Thus, the total length of the excavation in the design was 80 m. Moreover, shortening the excavation length can reduce the dimension of the 3D model, saving computational time and cost without affecting the numerical results.

Ten construction phases were performed with the total of 5 excavations and 4 slabs as listed in Table 1. The groundwater table was initial set 2.0 m below the ground surface and lowered to 1.0 m below excavation surface at each excavation phase. The distance from the lateral boundaries of the model to the diaphragm wall in the excavation was 80 m, which was about four times the excavation

Table 2 Input parameter of Mohr-Coulomb using Undrained A and B analysis

Depth (m)	Consistency	γ (kN/m^3)	c' (kPa)	ϕ'	N	S_u (kPa)	E_{50} (kPa)	E'_{50} (kPa)	E' (kPa)
0-7.95	Soft	14	6	38	4	24	66619	57759	86638
7.95-9.95	Very stiff	18	46	41	21	126	70763	61352	92028
9.95-19	Hard	18	46	41	39	234	75366	65342	98013
19-22.5	Stiff	18	46	41	12	72	80593	69874	104811
22.5-24.5	Hard	18	46	41	34	204	82884	71860	107790
24.5-38.95	Very Stiff	18	46	41	22	132	90172	78179	117269

Note: m = 1.0; R_f = 0.9; v' = 0.3; v_{ur} = 0.2; E'_{50} = 0.867 E_{50} and E' = 1.5 E'_{50}

depth. Standard fixed conditions were used to the FE model; horizontal movement was fixed at the lateral boundaries, and both horizontal and vertical movements were fixed at the bottom boundary of the model. The soil model, structural elements (diaphragm walls and floor slabs), and soil-structure interface elements are discussed in the following Section.

3.2 Input parameter

3.2.1 Soil parameter

Mostly, previous researchers in Indonesia often used plasticity index (PI) correlations to obtain the effective friction angle for Central Jakarta clay as shown in Figure 10 that was conducted by Bjearum and Simons. (1960). This concept is applicable for soft clay, but misleading with the Central Jakarta clay which possibly gives the underestimated value of strength parameter. Moreover, establishing the correlation value of soil stiffness corresponding to the depth has to be appropriate to achieve the better result compared with field measurement.

In this research, Hardening Soil (HS) result was compared with Mohr-Coulomb to evaluate the effective soil strength used in Undrained A with previous research conducted by Hsiung *et al.* (2018) using Undrained B performed by Plaxis 3D. Table 3 shows the input soil parameters in the HS model for the FE analyses. The soil strength is divided into two layers. The upper layer performed with 6 kPa of effective cohesion and 38° of effective friction angle obtained from high-quality of CU test. The lower layer used 46 kPa of effective cohesion and 41° of effective friction angle. The effective stress analysis under undrained conditions was simulated to model the short-term undrained conditions of the clay during the excavation process. The assumption of soil undrained conditions can be selected by low soil permeability, as described previously. Moreover, the real construction revealed that no pumping required, which is suggested that the soil in the research remained soil to undrained conditions.

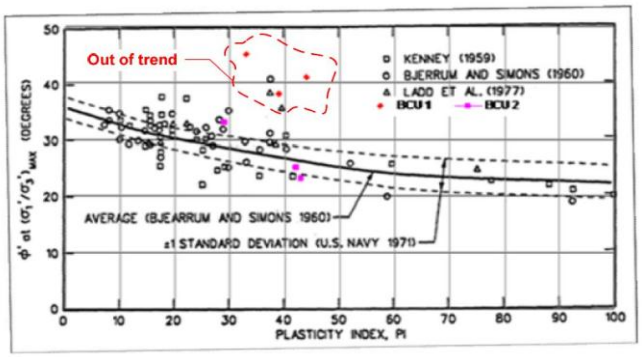

Figure 10 Relationship between plasticity index and effective friction angle (Bjearum and Simons 1960)

Two undrained functions, namely Undrained (A) and Undrained (B), were specified in Plaxis 3D: Undrained (A) requires effective stress parameters for both soil modulus and shear strength, whereas Undrained (B) is performed using the effective soil modulus and undrained soil shear strength.

The explanation of the undrained soil shear strength was discussed in Section 2.3.2. The numerical analyses results were performed using PMT as shown in Eq. (5) were compared with field measurement wall deformation

As noted, in the Plaxis 3D manual, when selecting Undrained B, the soil modulus in HS model becomes stress-independent. It is entirely different with Undrained A which needs to convert the value of the drained reference soil modulus (E_{50}^{ref}) by Eq. (7).

$$E'_{50} = E_{50}^{ref} \left(\frac{c' \cos\phi' + \sigma'_3 \sin\phi'}{c' \cos\phi' + P^{ref} \sin\phi'} \right)^m \quad (7)$$

Therefore, E′$_{50}$ can be used directly as E_{50}^{ref} in the Undrained B model because the value of effective soil strength becomes meaningless. However, the stress dependency of the soil modulus was still modeled by manually inputting various soil modulus values for soil layers to consider the change of the soil modulus with depth. Table 3 lists the E_{50}^{ref} values used in the simulation. As known in the Mohr-Coulomb soil model which only has a single soil modulus value that can be estimated to be E'_{50}= *1.5 E′* in this model. The HS model allows to input separate soil modulus values to distinguish the soil behavior under loading and unloading conditions. According to Lim *et al*. (2010) and Calvello and Finno. (2004), the reference modulus for unloading/reloading and oedometer loading were estimated to be $E_{ur}^{ref} = 3E_{50}^{ref}$ and $E_{oed}^{ref} = 0.7E_{50}^{ref}$. Similar procedures were suggested by Surarak *et al*. (2012) to determine input soil parameters in the HS model. Moreover, the sensitivity of each parameter on the wall deformation of an excavation was discussed by Gebreselasse and Kemfert. (2005).

3.2.2 Structural properties and interface elements

The retaining wall was 1.0 m thick and 24.2 m deep as built in the structure design. Corresponding to the American Concrete Institute, Young's modulus of concrete (E_c) can be obtained as follows:

$$E = 4700 f_c' \text{ (MPa)} \quad (8)$$

Where f'_c (MPa) is the standard compressive strength of the concrete. Considering the overlapping of unit weight and volume between soils and other materials (e.g., concrete and steel), the soil unit weight should be reduced in both of concrete and steel materials. Ou. (2006) suggested the stiffness (*EI*) of a diaphragm wall is usually reduced by approximately 20–40% to consider defects and cracks in the concrete. Therefore, 70% of wall stiffness was applied.

Table 3 Input parameter of Hardening Soil using Undrained A analysis

Depth (m)	Consistency	γ (kN/m³)	c' (kPa)	ϕ'	N	E_{50} (kPa)	E'_{50} (kPa)	E_{50}^{ref} (kPa)	E_{oed}^{ref} (kPa)	E_{ur}^{ref} (kPa)
0-7.95	Soft	14	6	38	4	66619	57759	287650	201355	862949
7.95-9.95	Very stiff	18	46	41	21	70763	61352	126885	88820	380655
9.95-19	Hard	18	46	41	39	75366	65342	111639	78147	334917
19-22.5	Stiff	18	46	41	12	80592	69874	99693	69785	299079
22.5-24.5	Hard	18	46	41	34	82883	71860	95616	66931	286848
24.5-40	Very Stiff	18	46	41	22	90172	78179	85654	59958	256963

Note: m = 1.0; R_f = 0.9; v' = 0.3; v_{ur} = 0.2 and E'_{50} = 0.867 E_{50}

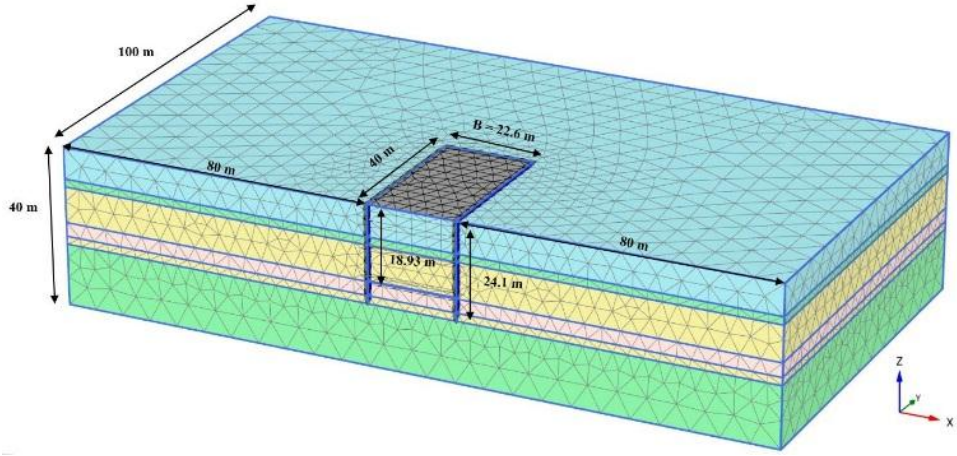

Figure 11 3D Finite element model of benchmark analysis

Table 4 shows the input material properties of the diaphragm wall used in Plaxis 3D. According to Ou. (2006), the axial stiffness of floor slabs in the top-down construction method must also be reduced by 20% of the total stiffness considering the construction process. This is because the compressive strength of the constructed concrete might differ from the design strength during the construction; defects and cracks in the concrete can also be considered through this approach. The slab thickness for each floor level and the parameters for the slabs are listed in Table 5.

Table 4 Input parameter of diaphragm wall

Parameter	Symbol	Value	Unit
Compressive strength of concrete	*f'c*	21	Mpa
Thickness	*d*	1	m
Young's modulus	*E*	21700	Mpa
Young's modulus 70%	*70%E*	15200	Mpa
Unit weight	γ	6	(kN/m³)
Poisson's ratio	*v*	0.15	-

Table 5 Input parameter of concrete slabs

Slabs	*d* (m)	*v*	80%*E* (MPa)
Deck slab	0.4	0.15	17400
Top slab	0.8	0.15	17400
Middle slab	0.4	0.15	17400
Bottom slab	1	0.15	17400

Plaxis 3D has the interface menu to design the plate elements. Interface elements were used to model the correlation between the soil and structural elements such as the diaphragm wall and bottom concrete slab. The value of the interface reduction factor (R_{inter}) influences both the stiffness and strength of the interface. According to Ou. (2006), R_{inter} = 0.67 is a typical value for the interface between clay and concrete interface.

4. RESULTS AND DISCUSSIONS

4.1 Comparison of prediction and field measurement

Figure 12 describes the comparisons of the measured and predicted wall from several soil constitutive models included HS Undrained A, HS Undrained B, MC Undrained A and MC Undrained B. Central Jakarta excavation was selected to model the simulation and it is located in the plane-strain condition as shown in Figure 3.

As displayed in Figure 12, the wall deformation kept raising corresponding to the excavation phase until reaching the maximum value in the last stage of the excavation. The comparison indicates that the input parameter used performed well to all soil constitutive models. However, the 3rd excavation shown in Figure 12 (c) describes that the numerical analysis was overestimated compared with field measurement data. Numerical analysis results in 5th excavation as displayed Figure 12 (d) are located between the field measurement data both sides (DW-15 and DW-171).

The predicted wall deformation for soil near wall toe of HS results was lesser than MC in the below of excavation zone because the stiffness moduli in the HS could take the elastic unloading process due to the excavation process by E_{ur}^{ref} together with comparatively short embedded wall depth. Moreover, the simulation results of

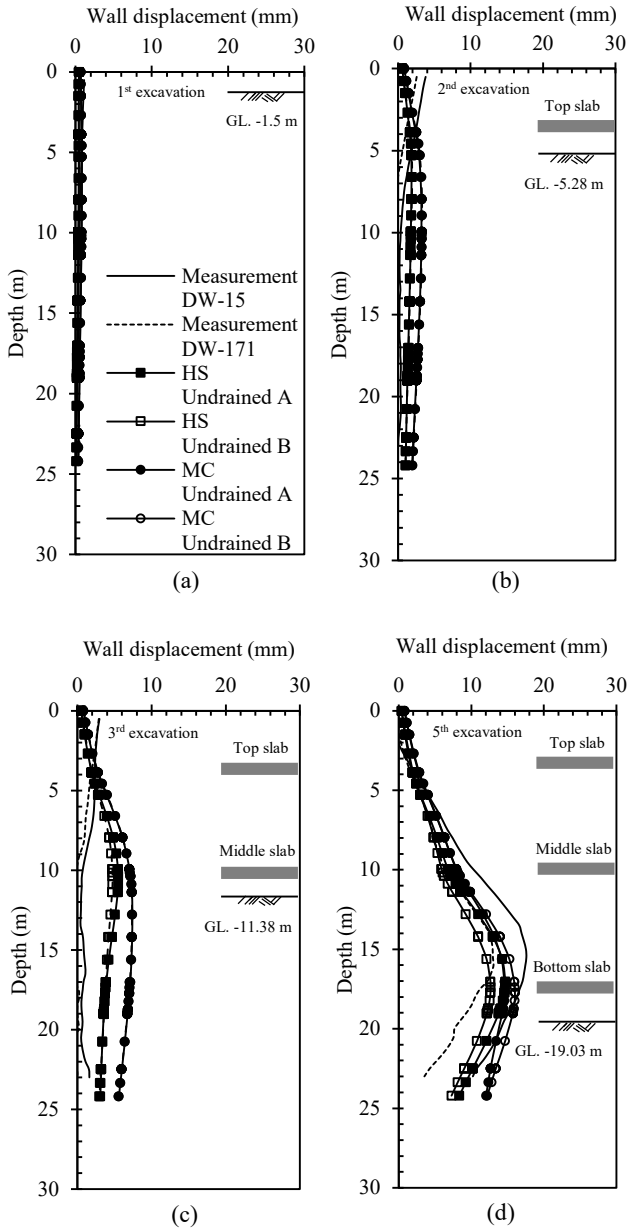

Figure 12 Comparison of predicted and measured wall displacement from several soil constitutive models at the excavation at various excavation stages: (a) 1st stage; (b) 2nd stage; (c) 3rd stage; (d) 5th (final excavation) stage

Undrained A for both HS and MC recorded the consistent result and located in the between of measurement data which mean the effective soil strength and total stress parameter are similar and further discussion will be carried out in the later section.

Figure 13 shows the shading of relative shear stress for each excavation process. The relative shear stress is the ratio of the mobilized shear strength and the maximum shear strength which illustrates the proximity of the stress point to failure envelope. The figure used MC Undrained A to see the evolution of relative shear stress in different phases. The shading of relative stress at 1st stage represented if the wall had no experience of high ground pressure against the wall as shown in Figure 13 (a). The transformation occurred in Figure 13 (b) and (c) which the wall has taken on the soil pressure. Eventually, in Figure 13 (d) indicates that the soil elements around the excavation site and the embedded length of diaphragm wall in plane-strain location became critical in the design of the numerical analysis.

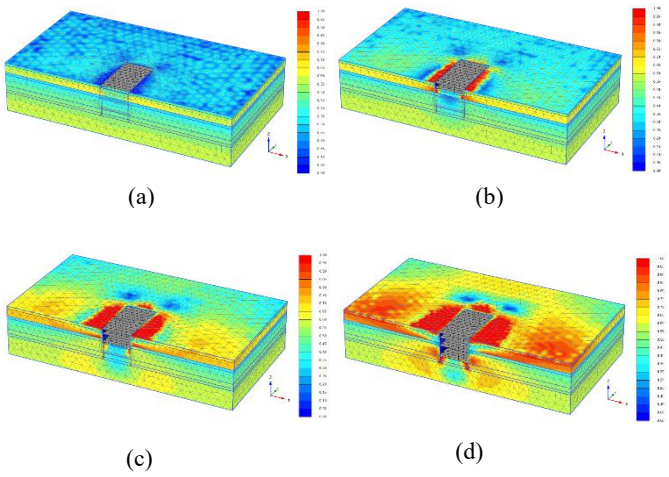

Figure 13 The shading of relative stress at different excavation stages from MC Undrained A: (a) 1st stage; (b) 2nd stage; (c) 3rd stage; (d) 5th (final excavation) stage

4.2 Stress path

The soil effective stress path (ESP) was conducted to learn the behavior of soil nearby the excavation location. The location of ESP was pointed in several locations namely A, B, C, D, and E. Each point of the effective stress path was investigated at different excavation stage to observe the p'-q value. The Mohr failure envelope can be modified into p'-q diagram called K_f line which is a tangent line of the Mohr circles which as shown in Eq. 10.

Technically, the purpose of observing ESP is to study the influence of unloading process during excavation based on numerical analyses at every stage toward the soil strength. Eq. 8 and 9 can be rewritten regarding of the effective stress. Moreover, Eq. 10 can express the relationship between the K_f line and the Mohr failure envelope:

$$p' = \frac{(\sigma'_V + \sigma'_H)}{2} \text{ (kPa)} \quad (8)$$

$$q = \frac{(\sigma'_V - \sigma'_H)}{2} \text{ (kPa)} \quad (9)$$

$$\sin \phi' = \tan \psi \quad (10)$$

All those ESP points were taken at every excavation depth and the toe of diaphragm wall as shown in Figure 14. Each point was observed for every stage of excavation. Points E and F were observed at the end of the embedded wall to represent the effective stress path because in the last excavation process, shown in Figure 13 (d), illustrates the highest stress occurred.

The stress path values are corresponding to the location of excavation depth and stress path points. The K_f line was obtained by the high-quality data of effective strength. When the stress path points are above the excavation depth, then the value of overburden stress would increase and would be in reverse when the stress path points under the excavation depth as shown in Points A, B, and C. Those are due to the horizontal stresses σ_H in the retaining zone decreases when the soils are excavated above the stress points and σ_H should increase when the soils are excavated below the stress path points. Moreover, in the point E shows that the overburden pressure increases corresponding to the excavation stages due to unloading process.

Figure 15 indicates that those values, based on numerical analysis results, were located below the K_f line and far enough to reach the K_f line which indicates that the models were in the safe zone and appropriate for the structure design. This indicates that by having a high-quality data of effective strength parameter and selecting stiffness moduli are necessary to obtain the consistent simulation

results of Undrained A and Undrained B, respectively. However, unless having a good quality test result, relative loading between soil stress status and failure envelope may not be the same which could lead totally different results from Undrained A and Undrained B analyses. Then, HS model with Undrained B analysis still can give acceptable results and it means as long as a set of proper soil stiffness can be given, HS model with total stress parameter can give a reasonable result.

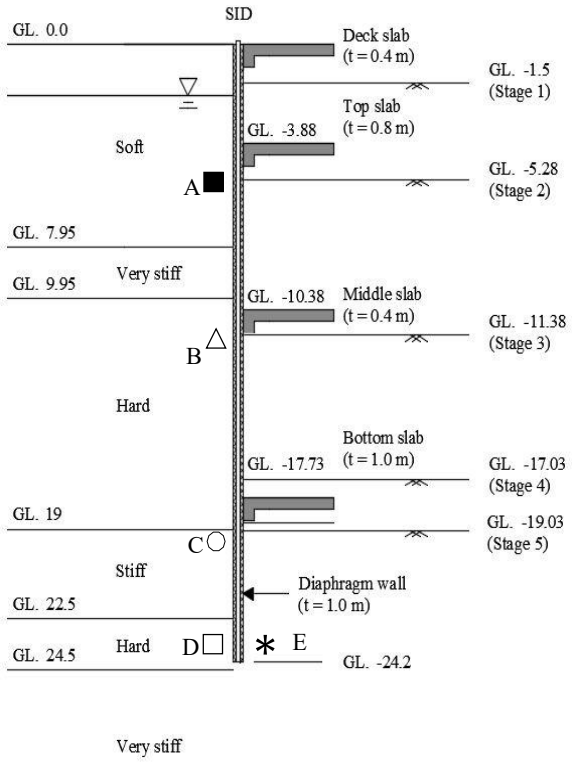

Figure 14 The location of selected stress points

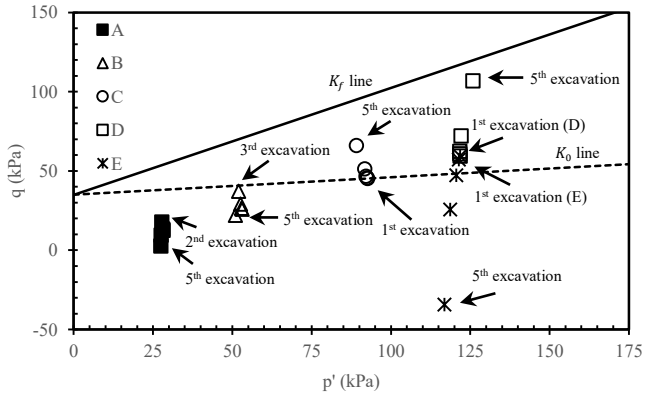

Figure 15 The effective stress path at the excavation area

4. CONCLUSIONS

This paper presents a case study and numerical simulations for a large-scale deep excavation to obtain the reliable total and effective soil strength based on the comparison of wall deformation between predicted and measured results in Central Jakarta excavation, Central Jakarta, Indonesia. Various soil constitutive models were established in numerical simulations included Hardening Soil Undrained A and B and Mohr-Coulomb Undrained A and B. Thereafter, the effective stress path was conducted to check the behavior of Central Jakarta clay during the excavation process. The following conclusions were illustrated by the results of this research:

1. The ground condition in Central Jakarta generally dominated by clay/silt which consisted of soft clay to very stiff clay. The natural water content of the clay in the range of 34.6 to 89.3% with LI of between 0.19 and 0.65. The SPT-N values were lower than 10 to a depth of 7 m (soft clay) and continuously in the average of 30 at depth 20 m (stiff clay).
2. The soil model was separated into upper soil layer and lower soil layer to simplified the input soil parameter. The upper layer performed with 6 kPa of effective cohesion and 38º of effective friction angle. Moreover, the lower layer used 46 kPa of effective cohesion and 41º of effective friction angle.
3. For Central Jakarta clay, a linear relationship between the soil modulus (from PMT) and depth was suggested to use $E_{50} = 833$ (z+76), were measured in kilopascals and meters. This empirical equation results were located in between of soil moduli obtained based on 2400N and 4000N.
4. The results of numerical analyses were compared between predicted and measured. The results indicate that the effective soil strength parameter used in Undrained A was reliable to be used in the analysis because the wall deformation results of predicted, located close to both sides of measurement data and Undrained B, were consistently good in numerical performance.
5. The stress path was conducted to confirm the result of diaphragm wall in the excavation site. The effective stress path points based on numerical results were located below the K_f line indicate that Undrained A and Undrained B could be performed equally well to be used.

Eventually, the effective (Undrained A) and total (Undrained B) shear strength properties results show that they could be performed and selected equally well to design the deep excavation in Central Jakarta. However, considering the high-quality data of effective soil strength and selecting soil Young's modulus are fundamental to obtain the rational result.

5. REFERENCES

Architectural Institute of Japan, 2001. Recommendations of Design of Building Foundation. Japan (in Japanese).

Calvello, N., Finno, R., 2004. Selecting parameters to optimize in model calibration by inverse analysis. Comput. Geotechn. 31, 410–424.

Gebreselessie, H., Kempfert, G., 2005. Sensitive study of the hardening soil model parameters based on idealized excavation. In: Proceedings of 11th International conference on computer methods and advances in geomechanics, Torino, Italy, pp. 321–328.

Hettiarachchi, H., Brown, T., 2009. Use of SPT blow counts to estimate shear strength properties of soils: energy balance approach. J. Geotechn. Geoenviron. Eng. 135 (6), 830–834.

Houston, W.N., Mitchell, J.K., 1969. Property interrelationships in sensitive clays. ASCE. J. Soil Mech. Found. Divis. 95 (4), 1037–1062.

Hsieh, P.G., Ou, C.Y., Lin, Y.K., Lu, F.C., 2015. Lessons learned in design of an excavation with the installation of buttress walls. J. GeoEng. 10, 67–73.

Hsiung, B.C.B., Hwang, R.N., 2009. Evaluating Performance of Diaphragm Walls by Wall Deflection Path. SEAGS. Special Issue on Excavation and Tunneling in Geotechnical Engineering, pp. 81–90.

Hsiung, B.C.B., Wang, C.L., Lin, H.T., Chen, C.H., 2013. Design and performance of a large scale excavation adjacent to sensitive structures in urban area. In: Proceedings of the 2nd International Conference on Geotechnics for Sustainable Development-Geotec. Hanoi 2013, Hanoi, Vietnam.

Hsiung, B.C.B., Yang, K.H., Aila, W., Hung, C., 2016. Three-dimensional effects of a deep excavation on wall deflections in loose to medium dense sands. Comput. Geotechn. 80, 138–151.

Hsiung, B.C.B., Yang, K.H., Aila, W., Ge, L., 2018. Evaluation of the wall deflection of a deep excavation in Central Jakarta using three-dimensional modeling. Tunnelling and Underground Space Technology. 72 (2018) 84-96.

Hwang, R.N., Moh, Z.C., 2007. Deflection paths and reference envelopes for diaphragm walls in the Taipei Basin. J. GeoEng. 1, 1–12.

Jaky, J., 1944. The coefficient of earth pressure at rest. J. Soc. Hungarian Archit. Eng. Budapest Hungry 355–358.

Kulhawy, F.H., Mayne, P.W., 1990. Manual on Estimating Soil Properties for Foundation Design. Electric Power Research Institute, Palo Alto, California.

Lim, A., Ou, C.Y., Hsieh, P.G., 2010. Evaluation of clay constitutive models for analysis of deep excavation under undrained conditions. J. GeoEng. 5, 9–20.

Lim, A., Ou, C.Y., 2017. Stress paths in deep excavations under undrained conditions and its influence on deformation analysis. Tunnelling and Underground Space Technology. 63 (2017) 118-132.

Likitlersuang, S., Surarak, C., Wanatowski, D., Oh, E., Balasubramaniam, A., 2013. Finite element analysis of a deep excavation: A case study from the Bangkok MRT. Soils Foundat. 53 (5), 756–773.

Mayne, P., Kulhawy, F.H., 1982. K0-OCR relationships in soil. J. Geotechn. Eng. Divis. 108 (GT6), 851–872.

Moh, Z.C., Hwang, R.N., 2005. Geotechnical considerations in the design and construction of subways in urban areas. Seminar on recent developments on mitigation of natural disasters, urban transportation and construction industry, Jakarta, Indonesia.

Muir-Wood, A., 1983. Index properties and critical state soil mechanics. Paper presented at the Proceeding of the Symposium on Recent Developments in Laboratory and Field Tests and Analysis of Geotechnical Problems, Bangkok, Thailand.

Ou, C.Y., Chiou, D.C., Wu, T.S., 1996. Three-dimensional finite element analysis of deep excavations. J. Geotechn. Eng. 122 (5), 337–345.

Ou, C.Y., Shiau, B.Y., Wang, I.W., 2000. Three-dimensional deformation behavior of the Taipei national enterprise center (TNEC) excavation case history. Canad. Geotechn. J. 37 (2), 438–448.

Ou, C.Y., 2006. Deep Excavation: Theory and Practice. Taylor & Francis, Netherlands.

Schweiger, H.F., 2009. Influence of constitutive model and EC7 design approach in FEM analysis of deep excavations. In: Proceedings of ISSMGE International Seminar on Deep Excavations and Retaining Structures, Budapest, Hungary, pp. 99–114.

Surarak, C., Likitlersuang, S., Wanatowski, D., Balasubramaniam, A., Oh, E., Guan, H., 2012. Stiffness and strength parameters for hardening soil model of soil and stiff Bangkok clays. Soils Foundat. 52 (4), 682–697.

Wang, J.H., Xu, Z.H., Wang, W.D., 2010. Wall and ground movements due to deep excavations in Shanghai soft soils. J. Geotechn. Geoenviron. Eng. 136, 985–994.

Yang, K.H., Uzuoka, R., Thuo, J.N., Lin, G.L., Nakai, Y., 2017. Coupled hydro-mechanical analysis of two unstable unsaturated slopes subject to rainfall infiltration. Engineering Geology. 216 (2017) 13-30.

Yong, K.Y., 2015. Learning lessons from the construction of Singapore Downtown line (DTL). In: Proceedings of International Conference and Exhibition on Tunneling and Underground Space, Kuala Lumpur, Malaysia.